Journal of Alloys and Compounds 511 (2012) 262–267

Contents lists available at SciVerse ScienceDirect

Journal of Alloys and Compounds

journal homepage: www.elsevier.com/locate/jallcom

Experimental investigation of the Ce–Cu phase diagram

Huaiying Zhou, Chengying Tang*, Minmin Tong, Zhengfei Gu, Qingrong Yao, Guangfei Rao

School of Materials Science and Engineering, Guilin University of Electronic Technology, Guilin, Guangxi 541004, PR China

ARTICLE INFO

Article history:
Received 28 April 2011
Received in revised form
18 September 2011
Accepted 19 September 2011
Available online 22 September 2011

Keywords:
Ce–Cu
X-ray diffraction
Thermal analysis
Phase diagram

ABSTRACT

The binary Ce–Cu system has been re-investigated via the selected eighteen key alloys by means of the differential scanning calorimetry (DSC), X-ray diffraction (XRD), and scanning electron microscopy (SEM) with energy dispersive X-ray analysis techniques. Five intermetallic compounds, Cu_6Ce, Cu_5Ce, Cu_4Ce, Cu_2Ce, and CuCe, have been confirmed. Cu_6Ce and Cu_2Ce melt congruently at 947 °C and 810 °C, respectively. Cu_5Ce, Cu_4Ce, and CuCe are formed through peritectic reactions, $L + Cu_6Ce \leftrightarrow Cu_5Ce$ at 799 °C, $L + Cu_5Ce \leftrightarrow Cu_4Ce$ at 792 °C, and $L + Cu_2Ce \leftrightarrow CuCe$ at 492 °C, respectively. Three eutectic reactions, $L \leftrightarrow (Cu) + Cu_6Ce$ at 879 °C, $L \leftrightarrow Cu_4Ce + Cu_2Ce$ at 753 °C, and $L \leftrightarrow CuCe + (\gamma Ce)$ at 407 °C, have been observed. One catatectic reaction, $(\delta Ce) \leftrightarrow L + (\gamma Ce)$ at 702 °C, was determined. According to the present experimental results, the Ce–Cu phase diagram is revised.

1. Introduction

The bulk metallic glasses (BMGs) have attracted much attention due to the unique properties and potential applications as functional materials [1–9]. The Ce–Cu system is one of the sub-systems of the Ce-based bulk metallic glasses with an exceptionally low glass transition temperature [4,10]. In order to improve the capability of predicting the glass formation ability of metallic glass alloys, knowledge of the accurate phase diagrams and thermodynamic properties of the Ce-based alloy systems is necessary. For example, information on the eutectic reactions and thermodynamic quantities of the liquid phase is critical for the evaluation of the glass forming regions in the metallic glass alloys. Therefore, a research project to construct a thermodynamic database of the Ce-based alloys via experiments and assessments is performed [11].

The Ce–Cu phase diagram was constructed firstly by Hanaman [12] through thermal analysis. However, the intermetallic compound Cu_5Ce was not reported [12,13]. This compound was reported firstly by Dwight [14] through lattice parameter measurements for a series of AB_5-type compounds. Later, Rhinehammer et al. [15] confirmed the existence of the hexagonal Cu_5Ce compound by means of electron microprobe of metallographic samples and X-ray analysis of single crystal. Cu_5Ce was then accepted in the Ce–Cu phase diagram [16]. Thus, although the phase boundaries of Ce–Cu liquid are in good agreement with each other [12,15,16], a disagreement appeared on the existence of Cu_5Ce.

Duisemaliev and Presnyakov [17] and Korolkov and Lysova [18] reported that the maximum solid solubility of Ce in Cu is close to 0.1 at.% on the basis of metallography, micro-hardness and electrical resistivity measurements. The maximum solid solubility of Cu in (γCe) and (δCe) is about 0.37 and 0.55 at.% [13], respectively. The currently accepted Ce–Cu phase diagram was evaluated by Subramanian and Laughlin [19].

Based on the literature review involving the measured phase diagram data [12–19], enthalpies of mixing of liquid alloys [20–22] and heat contents [23,24], the Ce–Cu system was optimized thermodynamically by Zhuang et al. [25] and Bo et al. [26]. Although the good agreement between the calculated and experimental phase diagram was claimed, the largest deviations between the calculated invariant reaction temperatures for the Ce–Cu system compare to the measured invariant reaction temperatures are 28 °C [25] and 14 °C [26], respectively. This difference is relatively too large to accept and may contribute to the experimental data. The purpose of the present work is to experimentally confirm the reason of this deviation, and establish an accurate Ce–Cu phase diagram for thermodynamic calculation in progress.

2. Experimental

Ce (99.9 wt.% purity) and Cu (99.9 wt.% purity) were used as starting materials. As described in the literature [27], the surface of Ce-rods were ground, polished, cleaned by ethanol and acetone and then kept in acetone before use. In the present work, eighteen alloys, which compositions (all in atomic fraction) were guided by the assessed phase diagram [19,25,26] and each with a total mass of about 2.0 g, were prepared to provide reliable phase diagram data over the whole composition range of the Ce–Cu system. The alloys were prepared by arc melting the pure elements in an atmosphere of high purity argon. The buttons were then inverted after each melting and melted five times to improve the homogeneity.

* Corresponding author. Tel.: +86 773 2291434; fax: +86 773 2290129.
E-mail addresses: csutcy@163.com, ctang@guet.edu.cn (C. Tang).

0925-8388/$ – see front matter © 2011 Elsevier B.V. All rights reserved.
doi:10.1016/j.jallcom.2011.09.054

Table 1
Invariant reaction in the Ce–Cu system.

Reaction	Composition of liquid (at.% Ce)	Temperature (°C)	Source
$L \leftrightarrow (Cu) + Cu_6Ce$	8.5	870	[12]
	8.5	876	[16]
	9.0	876	[15]
	8.8	892	[25]
	8.7	877	[26]
	9.0	879	This work
$L \leftrightarrow Cu_6Ce$	14.3	935	[12]
	14.3	938	[15]
	14.3	938	[25]
	14.3	937	[26]
	14.3	947	This work
$L + Cu_6Ce \leftrightarrow Cu_5Ce$	23.4	798	[15]
	25.7	799	[25]
	24.4	798	[26]
	23.3	799	This work
$L + Cu_5Ce \leftrightarrow Cu_4Ce$	23.5	796	[15]
	26.3	790	[25]
	24.6	796	[26]
	23.5	792	This work
$L \leftrightarrow Cu_4Ce + Cu_2Ce$	26.3	755	[12]
	26.3	756	[16]
	26.0	756	[15]
	26.8	784	[25]
	26.9	770	[26]
	26.0	753	This work
$L \leftrightarrow Cu_2Ce$	33.3	820	[12]
	33.3	817	[15]
	33.3	817	[25]
	33.3	816	[26]
	33.3	810	This work
$L + Cu_2Ce \leftrightarrow CuCe$	62.6	515	[12]
	60.3	516	[16]
	60.0	516	[15]
	60.6	515	[25]
	57.4	514	[26]
	62.0	492	This work
$L \leftrightarrow CuCe + (\gamma Ce)$	72.0	415	[12]
	72.0	424	[15]
	73.0	427	[25]
	71.1	427	[26]
$(\delta Ce) \leftrightarrow L + (\gamma Ce)$	72.0	407	This work
	94.0	708	[15]
	95.8	726	[25]
	94.2	708	[26]
	94.0	702	This work

According to the literature [12–19,25,26], the liquid phase appears for the alloys annealed at above 516 or 424 °C in the Ce-rich part. In order to avoid the appearance of the liquid phase and achieve the equilibrium at the solid state, the alloys 1–11 and 12–18 sealed in evacuated silica tubes were annealed in a high precision diffusion furnace with ±2 °C accuracy for temperature measurement at 500 °C and 300 °C for 20 days, respectively, and finally quenched into an ice–water mixture.

Phase identification was performed by X-ray diffraction (XRD) using monochromatic Cu K_α radiation (Rigaku D/Max2500PC, Japan). After standard metallographic preparation, the microstructures of typical alloys were first examined by means of optical microscopy and then analyzed by scanning electron microscopy with energy dispersive X-ray (SEM/EDX) (JSM-5100LV, Japan) to microstructure observation and composition measurement. Differential scanning calorimetric analysis of annealed alloys were carried out using a NETZSCH STA 449 F3 Jupiter® system in an Al_2O_3 crucible under a flow of pure Ar atmosphere. The measurement was performed between room temperature and 1100 °C with a heating and cooling rate of 10 °C/min. In the temperature range examined, the accuracy of the temperature measurement was estimated to be ±1 °C. The transition temperatures for the invariant reaction were determined from the onset of the thermal effect during the heating step, and the peak temperature of the last thermal effect on heating was taken for the liquidus, as Liu et al. proposed [28].

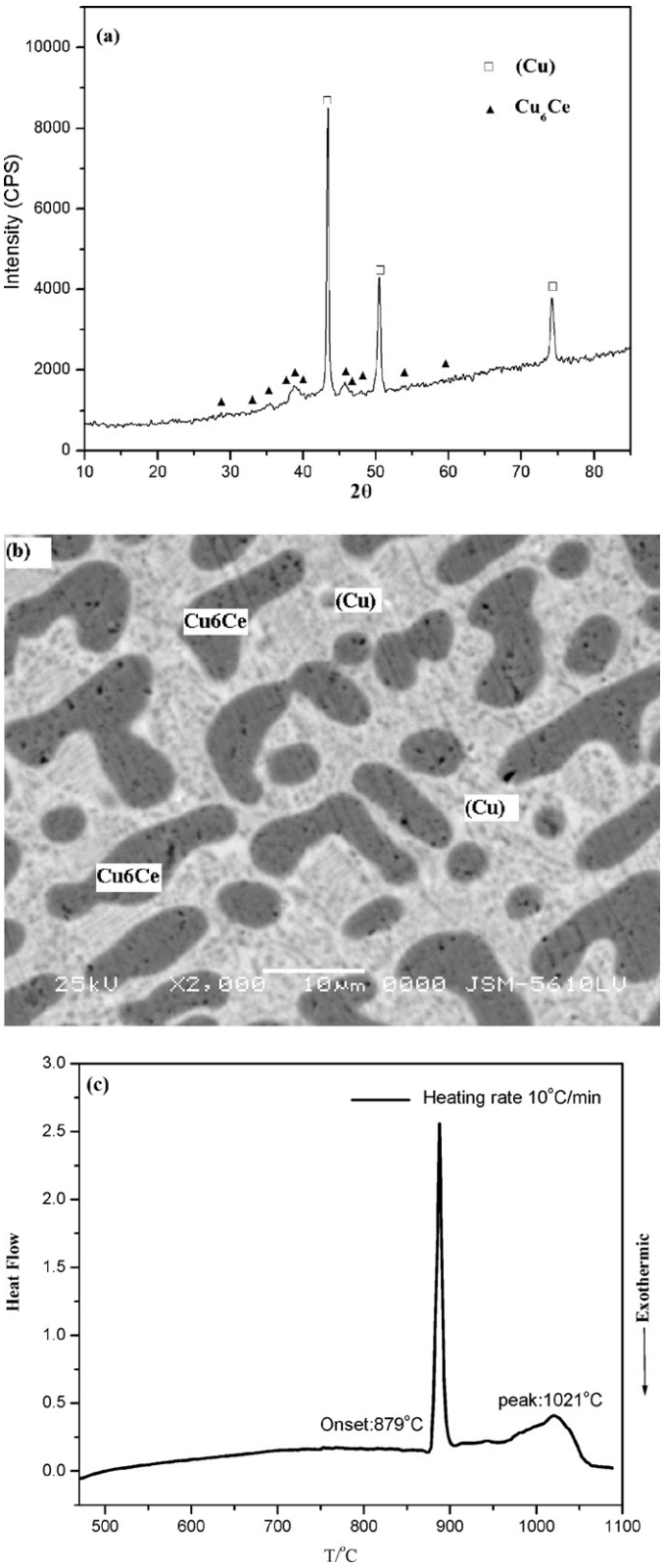

Fig. 1. XRD pattern (a), backscattered electron (BSE) image (b), and DSC curve with a heating rate of 10 °C/min (c) for the alloy 1 (Ce_5Cu_{95}) annealed at 500 °C for 20 days.

Table 2
Summary of the phases and phase transition temperatures for the samples in the Ce–Cu system.

No.	Ce (at.%)	Annealed condition	Phase	Transition temperature (°C)
1	5	500 °C, 20 days	(Cu) + Cu_6Ce	879.2, 1020.5
2	12	500 °C, 20 days	(Cu) + Cu_6Ce	880.4, 924.6
3	14.3	500 °C, 20 days	Cu_6Ce	879.3, 944.6
4	15	500 °C, 20 days	Cu_6Ce + Cu_5Ce	799.4, 879.0, 947.4
5	16.7	500 °C, 20 days	Cu_5Ce	792.4, 798.9, 879.3, 933.8
6	18	500 °C, 20 days	Cu_5Ce + Cu_4Ce	789.6, 805.8, 875.8, 918.3
7	20	500 °C, 20 days	Cu_4Ce	753.4, 788.3, 801.5, 882.9
8	22	500 °C, 20 days	Cu_4Ce + Cu_2Ce	753.6, 784.8, 808.1, 840.0
9	25	500 °C, 20 days	Cu_4Ce + Cu_2Ce	754.0, 766.6
10	30	500 °C, 20 days	Cu_4Ce + Cu_2Ce	752.0, 790.8
11	33.3	500 °C, 20 days	Cu_2Ce	752.6, 809.6
12	42	300 °C, 20 days	Cu_2Ce + CuCe	492.2, 765.1
13	50	300 °C, 20 days	CuCe	493.5, 692.4
14	58	300 °C, 20 days	CuCe + (γCe)	406.9, 493.1, 608.8
15	65	300 °C, 20 days	CuCe + (γCe)	406.8, 477.6
16	72	300 °C, 20 days	CuCe + (γCe)	408.3
17	80	300 °C, 20 days	CuCe + (γCe)	407.6, 509.3
18	97	300 °C, 20 days	CuCe + (γCe)	407.2, 701.6, 731.0

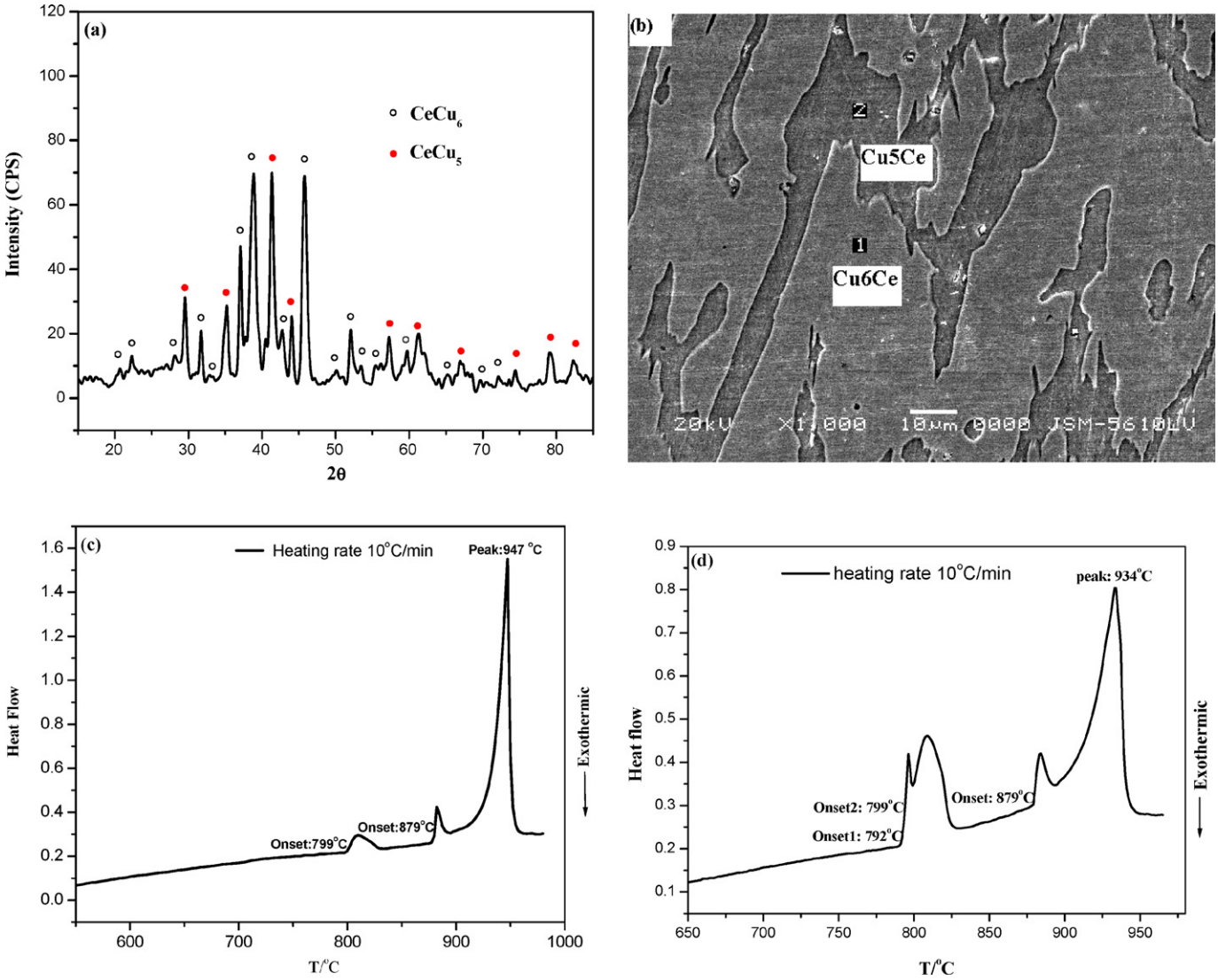

Fig. 2. XRD pattern (a), backscattered electron (BSE) image (b), DSC curve with a heating rate of 10 °C/min for alloys 4 ($Ce_{15}Cu_{85}$) (c) and 5 ($Ce_{16.7}Cu_{83.3}$), and (d) annealed at 500 °C for 20 days.

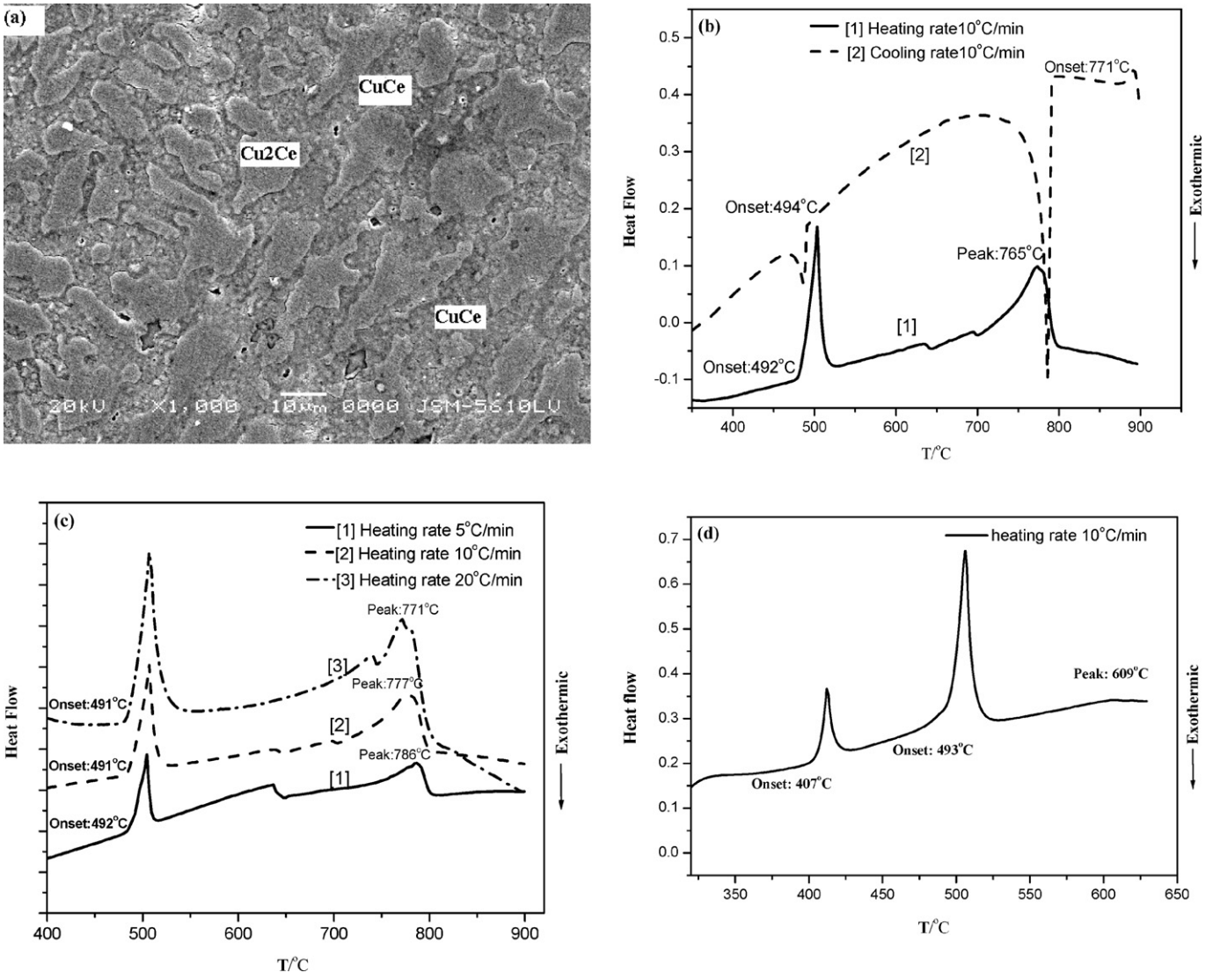

Fig. 3. Backscattered electron (BSE) image (a), DSC curves with a heating and cooling rate of 10 °C/min (b), DSC curves with a heating rate of 5, 10, and 20 °C/min for the alloy 12 ($Ce_{42}Cu_{58}$) (c), and DSC curve with a heating rate of 10 °C/min for the alloy 14 ($Ce_{58}Cu_{42}$) (d) annealed at 300 °C for 20 days.

3. Results and discussion

The invariant reaction temperatures measured from the DSC signals of the annealed alloys are given in Table 1 with the reported experimental and assessed values. Table 2 presents the phases identified by XRD, optical microscopy and SEM/EDX as well as phase transition temperatures obtained from DSC measurements. As can be seen in Table 2, five intermetallic compounds, Cu_6Ce, Cu_5Ce, Cu_4Ce, Cu_2Ce, and CuCe, were confirmed through XRD phase identification and microstructure observation.

From the DSC measurements for samples 1–3, it is indicated that the transition temperature for the invariant reaction $L \leftrightarrow (Cu) + Cu_6Ce$ is 879 °C. Fig. 1 shows the XRD pattern, backscattered electron (BSE) image, and DSC curve of the sample 1 (Ce_5Cu_{95}) annealed at 500 °C for 20 days. It is indicated that (Cu) and Cu_6Ce phases exist in this sample. As can be seen in Fig. 1c, the transition temperatures for the invariant reaction $L \leftrightarrow (Cu) + Cu_6Ce$ and liquidus are determined to be 879 °C and 1021 °C, respectively. This measured invariant reaction temperature is in good agreement with the previous experimental data (876 °C) [15] and the assessment (877 °C) performed by Bo et al. [26]. This result is disagreement with the assessed result (892 °C) performed by Zhuang et al. [25].

It is obtained from the DSC measurement for sample 4 ($Cu_{15}Ce_{85}$) that the transition temperature for the invariant reaction $L + Cu_6Ce \leftrightarrow Cu_5Ce$ is 799 °C. Fig. 2a–c presents the XRD pattern, backscattered electron (BSE) image, and DSC curve of sample 4 annealed at 500 °C for 20 days, respectively. It is found that this sample is composed of Cu_6Ce and Cu_5Ce compounds. The measured transition temperature of 799 °C (Fig. 2c) for the invariant reaction, $L + Cu_6Ce \leftrightarrow Cu_5Ce$, is in good agreement with the experimental value (798 °C) measured by Rhinehammer et al. [15] and calculated results (799 and 798 °C) by Zhuang et al. [25] and Bo et al. [26], respectively. This temperature is further confirmed by the DSC measurements for samples 5–8, although there is a little deviation existence due to this thermal effect has been covered by the first thermal effect for these samples. Fig. 2d shows the DSC curve of sample 5 ($Cu_{16.7}Ce_{83.3}$) annealed at 500 °C for 20 days. As indicated in Fig. 2d, the transition temperatures of 792 °C and 799 °C for the invariant reactions $L + Cu_5Ce \leftrightarrow Cu_4Ce$ and $L + Cu_6Ce \leftrightarrow Cu_5Ce$ are determined, respectively. This measured transition temperature of 792 °C for the invariant reaction is in good agreement

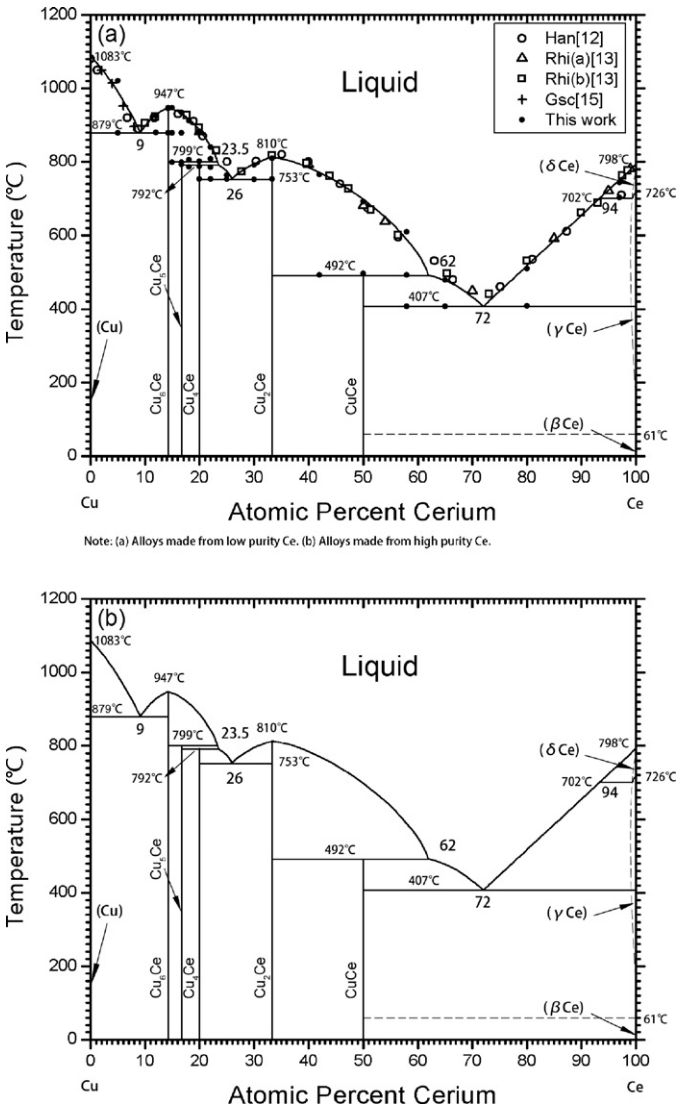

Fig. 4. The revised Ce–Cu phase diagram along with the experimental data from the present work and the literature (a) and without experimental data points (b).

with the measured 796 °C [15] previously and calculated results [25,26].

Note that one thermal effect on 879 °C, which corresponds to the invariant reaction L ↔ (Cu) + Cu_6Ce, has been detected for samples 4, 5 (Fig. 2c and d) and 6. This thermal effect detection for these two samples may contribute to the fact that the compound Cu_6Ce is not stoichiometric in composition at high temperature.

For the invariant reaction, L ↔ Cu_4Ce + Cu_2Ce, a large discrepancy between the measured temperatures (756 °C) [15,16] and calculated values (784 °C [25] and 770 °C [26]) is reported. In the present work, it is indicated from the DSC measurements for samples 7–11 that the transition temperature for this eutectic reaction is 753 °C. This measured result agrees well with the reported experimental temperature (756 °C) [15,16], and do not support the thermodynamic assessments of 784 °C [25] and 770 °C [26].

For the peritectic reaction, L + Cu_2Ce ↔ CuCe, the transition temperature was reported and evaluated to be 516 °C [12,15,19]. To confirm the transition temperature of this invariant reaction, samples 12–14 were prepared and examined. Fig. 3a–c presents the backscattered electron (BSE) image, DSC curves with a heating and cooling rate of 10 °C/min, DSC curves with a heating rate of 5, 10, and 20 °C/min for the sample 12 ($Ce_{42}Cu_{58}$), and DSC curve with a heating rate of 10 °C/min for the sample 14 ($Ce_{58}Cu_{42}$) annealed at 300 °C for 20 days. As can be seen in this figure, Cu_2Ce and CuCe were formed in this sample. However, the transition temperature for the peritectic reaction, L + Cu_2Ce ↔ CuCe, is determined to be 492 °C from DSC heating curve and confirmed from DSC cooling curve (Fig. 3c), which has 24 °C lower than the value reported [12,15] and evaluated by Subramanian and Laughlin [19]. DSC measurement of the sample 12 shown in Fig. 3d indicates that the transition temperature for invariant reaction is in good agreement with each other under different heating rates (5, 10, and 20 °C/min), except for the temperature for liquidus. Thus, the obtained equilibrium transition temperature for the invariant reaction, L + Cu_2Ce ↔ CuCe, by extrapolating the heating rate to 0 K is 492 °C. This indicates that the presently obtained invariant reaction temperature is reliable. Since Cu_2Ce is associated with these two invariant reactions, L ↔ Cu_4Ce + Cu_2Ce and L + Cu_2Ce ↔ CuCe, it is reasonably concluded that the large deviation of the calculated invariant reaction temperature of L ↔ Cu_4Ce + Cu_2Ce is attributed to the deviation from the measured invariant reaction temperature of L + Cu_2Ce ↔ CuCe.

To confirm the transition of the eutectic reaction L ↔ CuCe + (γCe), samples 14–18 were prepared and examined. As shown in Fig. 3d, it is indicated that the transition temperature for this eutectic reaction is 407 °C, which has 17 °C lower than the evaluated value [19]. The transition temperature of 492 °C for the peritectic reaction, L + Cu_2Ce ↔ CuCe, is further confirmed from Fig. 3d. Additionally, according to the present measurement, the temperature associated with the catatectic reaction (δCe) ↔ L + (γCe) is determined at 702 °C.

Accordingly, based on the experimental data obtained in the present work, Fig. 4 presents the revised Ce–Cu phase diagram with the experimental data from the present work and the literature. The revised phase diagram is expected to substitute for the currently accepted version and used for thermodynamic calculation in progress.

4. Summary

The Ce–Cu system was re-investigated using XRD, SEM and DSC techniques. Five compounds, Cu_6Ce, Cu_5Ce, Cu_4Ce, Cu_2Ce, and CuCe, were confirmed in this system. Cu_6Ce and Cu_2Ce are of congruent melting behaviors, while Cu_5Ce, Cu_4Ce, and CuCe are formed via peritectic reactions. Three eutectic reactions, L ↔ (Cu) + Cu_6Ce at 879 °C, L ↔ Cu_4Ce + Cu_2Ce at 753 °C, and L ↔ CuCe + (Ce) at 407 °C, three peritectic ones, L + Cu_6Ce ↔ Cu_5Ce at 799 °C, L + Cu_5Ce ↔ Cu_4Ce at 792 °C, and L + Cu_2Ce ↔ CuCe at 492 °C, and one catatectic reaction, (δCe) ↔ L + (γCe) at 702 °C, as well as two congruent melting behaviors, L ↔ Cu_6Ce at 947 °C and L ↔ Cu_2Ce at 810 °C, were examined. A revised Ce–Cu phase diagram is presented mainly based on the present experimental results.

Acknowledgements

The financial support from the National Natural Science Foundation of China (50861006) and the Natural Science Foundation of Guangxi (0991002Z, 2011GXNSFC018002) are greatly acknowledged.

References

[1] L. Xia, K.C. Chan, M.B. Tang, J. Alloys Compd. 509 (23) (2011) 6640–6643.
[2] H. Fu, M. Zou, J. Alloys Compd. 509 (13) (2011) 4613–4616.
[3] J.H. Han, N. Mattern, D.H. Kim, J. Eckert, J. Alloys Compd. 509 (S1) (2011) S42–S45.
[4] T. Wang, Y.Q. Yang, J.B. Li, G.H. Rao, J. Alloys Compd. 509 (13) (2011) 4569–4573.
[5] Q. Wang, J.M. Pelletier, J.J. Blandin, J. Alloys Compd. 504 (2010) 357–361.

[6] Z.Y. Liu, Y. Yang, S. Guo, X.J. Liu, J. Lu, Y.H. Liu, C.T. Liu, J. Alloys Compd. 509 (7) (2011) 3269–3273.
[7] A.A. Al-Ghamdi, M.A. Alvi, S.A. Khan, J. Alloys Compd. 509 (5) (2011) 2087–2093.
[8] Y. Ji, S. Pang, T. Zhang, J. Alloys Compd. 505 (2010) 497–500.
[9] L. Wu, S. Li, J. Fang, Q. Chen, K. Peng, J. Alloys Compd. 504 (2010) S38–S40.
[10] B. Zhang, D.Q. Zhao, M.X. Pan, W.H. Wang, A.L. Greer, Phys. Rev. Lett. 94 (2005) 205502.
[11] Q.R. Yao, X.D. Hu, X.J. Chen, S.K. Pan, W. Zou, H.L. Wang, Y.C. Wang, P.P. Wang, F. Liu, Z.M. Wang, H.Y. Zhou, C.Y. Tang, J. Alloys Compd. 484 (2009) 86–89.
[12] F. Hanaman, Int. Z. Metallogr. 7 (1915) 174–224.
[13] K.A. Gschneidner Jr., Rare Earth Alloys, D. Van Nostrand Co., Inc., Princeton, NJ, 1961.
[14] A.E. Dwight, Trans. ASM 53 (1961) 479–500.
[15] T.B. Rhinehammer, D.E. Etter, J.E. Selle, P.Z. Tucker, Trans. Metall. Soc. AIME 230 (1964) 1193–1198.
[16] K.A. Gschneidner Jr., M.E. Verkade, Selected Cerium Phase Diagrams Report IS-RIC-7, vol. 1, Rare-Earth Information Center, Energy and Mineral Resources Research Institute, Iowa State University, Ames, IA, 1974, pp. 8–19.
[17] U.K. Duisemaliev, A.A. Presnyakov, Zh. Neorg. Khim. 9 (1964) 2258–2260.
[18] A.M. Korolkov, E.V. Lysova, in: A.M. Korolkov (Ed.), Strukt. Svoistva Legk., Splavov, Nauka, Moscow, 1971, pp. 17–20.
[19] P.R. Subramanian, D.E. Laughlin, Bull. Alloy Phase Diagrams 9 (1988) 322–331.
[20] M.A. Turchanin, I.V. Nikolaenko, G.I. Batalin, Rasplavy 2 (1988) 25–28.
[21] K. Fitzner, O.J. Kleppa, Metall. Trans. A 24 (1993) 1827–1834.
[22] K. Fitzner, O.J. Kleppa, Metall. Mater. Trans. A 25 (1994) 1495–1500.
[23] W. Dokko, R.G. Bautista, Metall. Trans. B 11 (1980) 511–518.
[24] G.J. Qi, K. Itagaki, A. Yazawa, Mater. Trans. JIM 30 (1989) 273–282.
[25] W. Zhuang, Z.Y. Qiao, S. Wei, J. Phase Equilibr. 17 (6) (1996) 508–521.
[26] H. Bo, S. Jin, L.G. Zhang, X.M. Chen, H.M. Chen, L.B. Liu, F. Zheng, Z.P. Jin, J. Alloys Compd. 484 (1/2) (2009) 286–295.
[27] C.Y. Tang, Y. Du, L.J. Zhang, H.H. Xu, Z.J. Zhu, J. Alloys Compd. 437 (2007) 102–107.
[28] S.H. Liu, Y. Du, H.H. Xu, C. He, J.C. Schuster, J. Alloys Compd. 414 (2006) 60–65.